Eco-friendly gelatin films with rosin-grafted cellulose nanocrystals for antimicrobial packaging

Liliane S. F. Leite[a,b,c], Stanley Bilatto[b], Rafaella T. Paschoalin[c], Andrey C. Soares[b], Francys K. V. Moreira[d], Osvaldo N. Oliveira Jr.[c], Luiz H. C. Mattoso[a,b], Julien Bras[e,f]*

[a]Federal University of São Carlos, Graduate Program in Materials Science and Engineering (PPGCEM), 13565-905, São Carlos-Brazil, lilianesamara@gmail.com

[b]National Nanotechnology Laboratory for Agribusiness, Embrapa Instrumentação, XV de Novembro street, 1452, 13560–979, São Carlos-Brazil, stanleyebr@gmail.com, andreycoatrini@gmail.com luiz.mattoso@embrapa.br

[c]University of São Paulo, São Carlos Institute of Physics, 13560–970, São Carlos-Brazil, rafa.rrtp@gmail.com, chu@ifsc.usp.br

[d]Department of Materials Engineering, Federal University of São Carlos, Rod. Washington Luis, km 235, São Carlos (SP), 13565–905, Brazil. moreira.fkv@dema.ufscar.br

[e]University Grenoble Alpes, CNRS, Grenoble INP, LGP2, F-38400 Grenoble, France,

[f]Nestle Research Center, 1000 Lausanne, Switzerland

KEYWORDS. Gelatin; rosin; cellulose nanocrystal; antimicrobial properties; food packaging.

ABSTRACT

We report on gelatin films incorporating rosin-grafted cellulose nanocrystals (r-CNCs), which fulfill the most relevant requirements for antimicrobial packaging applications. Transparent gelatin/r-CNCs bionanocomposite films (0.5 – 6 wt% r-CNCs) were obtained by solution casting and displayed high UV-barrier properties, which were superior to the most used plastic packaging films. The gelatin/r-CNCs films exhibited a moderate water vapor permeability (0.09 g mm/m^2 h kPa), and high tensile strength (40 MPa) and Young's modulus (1.9 GPa). The r-CNCs were more efficient in improving the optical, water vapor barrier and tensile properties of gelatin films than conventional CNCs. Grafting of rosin on CNCs resulted in an antimicrobial nanocellulose that inhibited the growth of *Staphylococcus aureus* and *Escherichia coli*. The antibacterial properties of r-CNCs were sustained in the gelatin films, as demonstrated by agar diffusion tests and proof-of-principle experiments involving cheese storage. Overall, the incorporation of r-CNCs as active fillers in gelatin films is a suitable approach for producing novel eco-friendly, antimicrobial packaging materials.

GRAPHICAL ABSTRACT
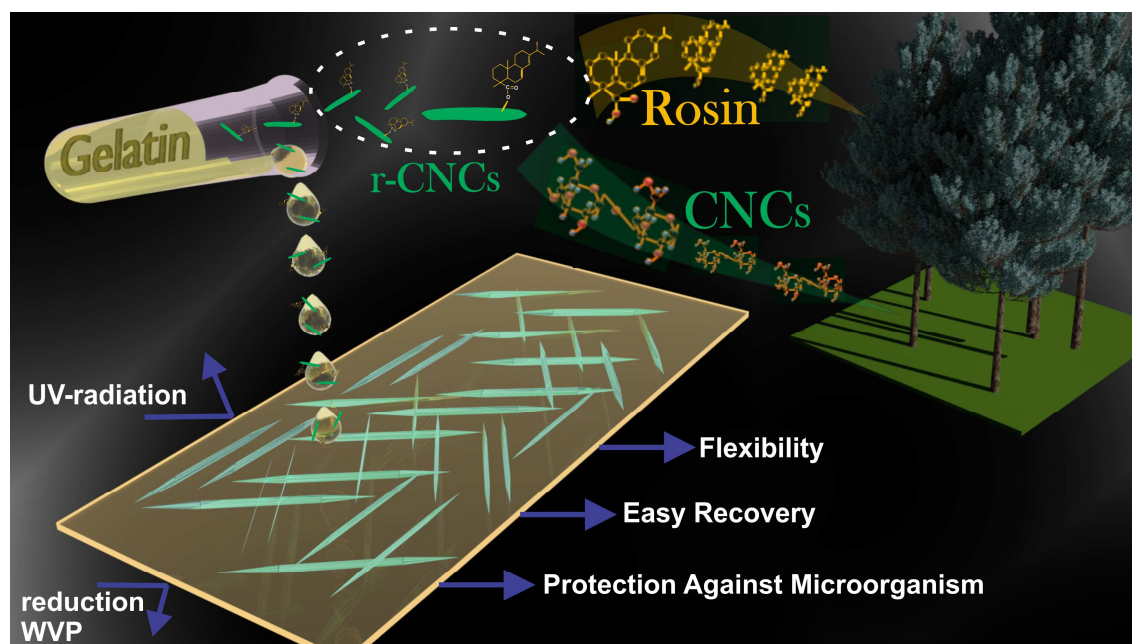
1. INTRODUCTION

Sustainability related to food plastic packaging has worldwide relevance owing to the need for safe disposal of post-consumer plastic wastes [1]. These problems can be mitigated if natural biodegradable polymers are employed as a packaging material, for which biopolymers have to exhibit suitable physical properties and increase the quality and safety of foods [2,3]. Desirable

43 properties of a packaging material include adequate mechanical strength, thermal stability,

44 recyclability, biodegradability, and barrier against water vapor and oxygen [4]. Research has been

45 focused on incorporating antimicrobial agents in packaging films to delay microbial growth [5],

46 which is the major cause of deterioration of foods [6]. This microbial growth may cause off-flavor

47 development, textural changes, loss of nutritive value, shelf-life reduction, increased risk of

48 foodborne illnesses [7], thus rendering the product unacceptable for human consumption [8].

49   Proteins such as gelatin can be suitable for food packaging due to their renewability,

50 biodegradability, low cost, film-forming ability, and edible nature [1,9,10]. Gelatin is a water-

51 soluble protein produced from partial hydrolysis of collagen, one of the most used biopolymers in

52 the food and pharmaceutical fields [11]. Gelatin films have suitable properties, such as

53 transparency, biodegradability, and low oxygen permeability [12], but they show poor barrier

54 properties against moisture and only moderate mechanical strength under high relative humidity

55 [13]. These drawbacks could be overcome by incorporating reinforcing nanoparticles, such as

56 cellulose nanocrystals (CNCs), in gelatin films [9,16–19]. CNCs are biodegradable, renewable, and

57 exhibit a low density, high elastic modulus (~150 GPa), and tensile strength (~7.5 GPa), being

58 produced in a commercial scale [20]. In addition to their use in polymer nanocomposites [21] to

59 enhance the physical properties of protein films [22–25], CNCs can also be chemically modified to

60 possess functionalities [26–29] such as antibacterial activity as with incorporation of titanium oxide

61 [30] and silver [31]. A limitation of this latter approach, however, is the toxicity of these metals that

62 could be released to the food [32]. This is motivation for the use of natural antimicrobial agents.

63   Rosin is an abundant natural product of pine resins, which is produced in more than 1

64 million tons annually [33,34] and contains a mixture of acids (ca. 90%) with hydrogenated

65 phenanthrene ring structures [35]. These acids are used in such applications as renewable feedstocks

66 for polymer synthesis due to their biodegradability and nontoxicity [33,34,36]. CNCs grafted with

67 natural rosin mixtures (r-CNCs) showed antimicrobial activity against Gram-negative and Gram-

positive bacteria [37]. Rosin-based bionanocomposites have been tested in active packaging films [38,39], but their preparation required chloroform or dichloromethane to disperse the polymer, limiting their application in the food industry.

Herein, rosin-grafted CNCs were synthesized and incorporated in gelatin films to enhance their physical properties for antimicrobial packaging. A systematic investigation was made to determine the effect of r-CNCs on the optical, water vapor and O_2 barrier and tensile properties of gelatin films, and the results are compared with those using conventional (non-grafted) CNCs. To the best of our knowledge, the use in food packaging of mechanically-reinforced gelatin films with antimicrobial properties remains unexplored. We demonstrate the potential of gelatin films loaded with r-CNCs with agar diffusion tests and storage experiments using mozzarella cheese as a model food matrix.

2. MATERIALS AND METHODS

2.1. Materials

Bovine gelatin powder (Bloom Strength-180) was kindly supplied by Gelco Gelatinas do Brazil Ltda (Pedreira, SP). CNCs, isolated from wood pulp by sulfuric acid hydrolysis and delivered as a dried powder, were purchased from Celluforce Inc. (Windsor, Québec, Canada). Rosin was purchased from Aldrich Chemical (USA). Glycerol and ethanol were purchased from Across Organics (USA). All chemicals were of analytical grade and were used as purchased. *Staphylococcus aureus* (*S. aureus*, Gram-positive, ATCC 25923) and *Escherichia coli* (*E. coli*, Gram-negative, ATCC 25922) were supplied by Cefar Diagnostica (Brazil). Distilled water was used in all experiments.

2.2. Synthesis of rosin-grafted CNCs (r-CNCs)

The CNCs were functionalized with rosin by a SolReact (solvent-free) process adapted from Castro et al.[37]. In this process, carboxylic acids are the solvent and grafting agents at the same time. The water evaporation during the reaction provokes an in situ solvent exchange from water to the reactant, which allows for efficient esterification according to Le Chatelier's principle, and saturation of CNCs with the melted carboxylic acid at low pH [40]. The reaction mechanism is presented in Fig. S1 in the Supporting Information. 2.0 g of CNCs were dispersed in water at 1.0 wt% and ultrasonicated for 2 min using a Branson sonicator, and the pH was adjusted to 4.0 with HCl (0.1 mol/L). The CNCs dispersion was placed in a closed distillation system in an oil bath at 130 °C. After 10 min, 22.35 g of rosin (10 equiv. according to the CNCs dry weight) were added slowly to ensure its melting and adsorption on the CNCs surface. The system was kept under stirring for 9 h at 130 °C. After the reaction, the rosin-grafted CNCs (r-CNCs) were purified from unreacted rosin by six dispersion-centrifugation cycles (10000 rpm at 4 °C for 10 min) with a large excess of ethanol, until no more rosin was detected by FTIR in the supernatant. Afterward, the r-CNCs were recovered by centrifugation and washed thoroughly with water, and then sonicated for 5 min and stored in a refrigerator. The final solid content was 3.5% (w/w).

2.3. Preparation of gelatin/r-CNCs bionanocomposite films

The bionanocomposite films were prepared by solvent casting. The gelatin powder was hydrated in distilled water (10 g/100 g) at 24 °C for 5 min and then heated at 60 °C under stirring for 15 min. Glycerol (20 wt% on a dry gelatin basis) was added to the gelatin solution under stirring. The solution obtained was mixed with the r-CNCs suspension at various contents (0 wt%, 0.5 wt%, 4.0 wt% and 6.0 wt%, on a dry gelatin basis) and stirred for 5 min. The suspensions (45 mL) were then cast on glass plates (40 × 25 cm) covered with a polyester film (Mylar®, DuPont, Brazil) to facilitate film peeling off after drying at room temperature for 24 h. Film samples were

117 conditioned at 50% RH and 25 °C for at least 24 h prior to testing. Gelatin films incorporated with

118 non-grafted CNCs were prepared at the same concentrations described above for comparison.

119

120 **2.4. Characterization**

121

122 **2.4.1. Structural and morphological analyses of r-CNCs**

123   The functionalization of CNCs with rosin was characterized by X-ray photoelectron

124 spectroscopy (XPS, XR3E2, Vacuum Generator, UK) equipped with monochromatic Mg Kα X-ray

125 source (1253.6 eV) operated at 15 kV and 20 mA. CNCs and r-CNCs were characterized by Fourier

126 Transform Infrared Spectroscopy (FTIR, FT-NIR VERTEX spectrometer, Bruker, Germany) in the

127 attenuated total reflection (ATR) mode. Spectra were recorded between 4000 and 400 cm^{-1} with a

128 resolution of 1 cm^{-1} and 32 spectral accumulations. The FTIR measurements of gelatin films were

129 carried out with five repetitions for each film sample. PVC films were also characterized to

130 compare the light transmission of the gelatin bionanocomposites with synthetic packaging films.

131 The morphology of CNCs and r-CNCs was investigated using transmission electron microscopy

132 (TecnaiTM G2 F20 microscope, FEI Company, USA) in the STEM (Scanning Transmission

133 Electron Microscopy) mode with an accelerating voltage of 80 kV. The samples were prepared by

134 depositing a 0.1 wt% suspension droplet on a carbon microgrid with formvar (400 mesh) stained

135 with 1.5 wt% uranyl acetate solution. A minimum of 10 images was recorded and the most

136 representative one was used for discussion. The CNCs and r-CNCs sizes were determined from the

137 analysis of a minimum of 100 particles using the ImageJ software.

138   The crystallinity of CNCs and r-CNCs was estimated by X-ray diffraction (XRD,

139 Panalytical diffractometer, X'Pert Pro MPD-Ray, The Netherlands) with Ni-filtered Cu Kα

140 radiation (λ = 1.54 Å, 45 kV, 40 mA) in the 2θ range from 5° to 60°. The crystallinity index (CI)

141 was calculated according to the Segal's equation [41]:

142      $CI\ (\%) = \left(1 - \frac{I_1}{I_2}\right) x100$ (1)

143

144   where I_1 is the intensity at the minimum ($2\theta = 18°$) and I_2 in the intensity associated with the

145   crystalline region of cellulose ($2\theta = 22.7°$).

146

147   **2.4.2. Morphological and optical analysis of CNCs and r-CNCs/gelatin films**

148   The film cross-sectional surface was studied using a JEOL Scanning Electron Microscope

149   (SEM, model Quanta200, FEI, the Netherlands). The samples were first cryo-fractured in liquid N_2

150   and then fixed onto 90° specimen mounts to be coated with a ca. 5-nm-thick gold layer in an argon

151   atmosphere. The SEM images were taken at accelerating voltages below 5 kV using the secondary

152   electron mode. Polarization-modulation infrared reflection-absorption spectroscopy (PM-IRRAS)

153   was conducted on a spectrophotometer (PMI 550, KSV Instruments, Finland). The light beam angle

154   of incidence was 81°. An average of 600 scans was collected for each spectrum at resolution of 8

155   cm^{-1}. In the PM-IRRAS technique, the incoming light is continuously modulated between *s*- and *p*-

156   polarization at a high frequency, so that the spectra for the two polarizations can be measured

157   simultaneously. Therefore, the films were placed on an Au substrate and the PM-IRRAs spectra

158   were obtained from the reflectivity components s and p, as given by Eq. 2:

159

160      $\Delta R/R = (R_p - R_s / R_p + R_s)$ (2)

161

162   where R_p is the reflectivity of the parallel component (*p*-polarization) and R_s is the reflectivity of

163   the component perpendicular to the light plane of incidence (*s*-polarization). All measurements

164   were carried out in a class 10,000 cleanroom at 23 ± 1 °C. Transmittance spectra were acquired in

165   triplicate on a UV-1650 spectrophotometer (Model PC, Shimadzu, Kyoto, Japan) at wavelengths

166   between 190 and 800 nm.

2.4.3. Water vapor and O$_2$ barrier and tensile properties determinations

The water vapor permeability (WVP) of the films was determined following ASTM E-96-01. The preconditioned film was sealed onto the opening of an aluminum permeation cup (28 mm internal diameter) containing dried calcium chloride. The cup was kept in a controlled chamber at 23 ± 1 °C and 50 ± 5% RH. The cup was weighed at least four times for at least 7 days under this controlled environment. For each film, three replicates were performed. WVP [(g mm)/ m^2 h kPa) was determined using Eq. 3:

$$WVP = WVTR \times L/\Delta p \tag{3}$$

in which WVTR is the water vapor transmission rate (g/m^2 h) through the film area; L is the film thickness (mm), and Δp is the partial pressure gradient (kPa) across the film.

The Oxygen Transmission Rate (OTR) of the films was determined in duplicate at 0%, 50%, and 80% RH according to the ASTM D3985 method (2002a) using an oxygen transmission rate analyzer (Systech Illinois 8500, USA). The tensile properties of the films were determined as per the ASTM D882-09 standard method (2009). Film specimens were prepared and equilibrated at 23 ± 1 °C and 50 ± 5% RH for 48 h. The tests were carried out on an Instron Universal Testing Machine (model 5569, Instron Corp., USA) with a 100 N load cell. The specimens were stretched using crosshead speed of 10 mm/min with clamps initially separated by 100 mm. Tensile strength, Young's modulus, and elongation at break were calculated from the stress-strain curves. The tests were performed with five replicates for each film. Film thickness was measured with a digital micrometer (Mitutoyo Corp., Kanogawa, Japan) to the nearest 0.001 mm. At least 10 specimens of each composition were analyzed.

2.4.4. Antimicrobial activity tests

192   The bacterial strains to evaluate the effectiveness of CNCs- and r-CNCs-loaded gelatin

193   solutions were *Staphylococcus aureus* and *Escherichia coli*, which are foodborne pathogens

194   [42,43]. The inoculum cultures were prepared inoculating a selected single colony in 15 mL of

195   Muller-Hinton Broth medium (MHB), followed by overnight incubation at 35 °C. The optical

196   densities at 625 nm were measured by UV-Vis absorption spectroscopy and compared with the

197   turbidity of a 0.5 McFarland standard at the same wavelength, equivalent to 1.5×10^8 colony

198   forming units per mL (CFU/mL). The overnight cultures were diluted in MHB until reaching 10^6

199   CFU/mL. The antimicrobial activity of the CNCs and r-CNCs suspensions was assessed by

200   determining the minimum inhibitory concentration (MIC) in a 96 flat-bottomed-well tissue culture

201   microplate. Briefly, 100 μL of sterile Mueller Hinton were added to all wells. In the first column,

202   the wells were filled with 50 μL of CNCs (50 mg.ml^{-1}) and r-CNCs (22 mg.ml^{-1}) suspensions. Then,

203   50 μL of each antimicrobial substance were serially transferred from the well to the corresponding

204   wells. Then, 50 μL of the culture suspension were added to all wells. Positive and negative controls

205   (streptomycin and culture medium – data not shown) were included in each assay plate. Afterward,

206   the inoculated plates were incubated in a wet chamber for 24 h at 35 °C and then chlorinated with

207   50 μL of 2,3,5$^-$Triphenyltetrazolium chloride (0.1%). The lowest sample concentration with an

208   inhibition effect on microbial growth was considered as the MIC for each tested microorganism. In

209   the antimicrobial film test, all films were cut into discs of 10 mm diameter and both sides were

210   sterilized by UV treatment in a laminar flow hood for 30 min. The discs were placed on Muller-

211   Hinton Agar (MHA) plates that had been previously seeded with 100 μL of inoculums containing *S.*

212   *aureus* or *E. coli* at a concentration of 1×10^6 CFU/mL. The plates were then incubated at 35 °C for

213   24 h. Two independent experiments were performed in triplicate. The antibacterial activity of the

214   gelatin/r-CNCs films on mozzarella cheese was also investigated. Fresh mozzarella samples (20

215   mm x 20 mm x 10 mm; four replicates) were wrapped with gelatin and gelatin/r-CNCs films. All

216 samples were packaged, sealed and stored at room temperature for 1 month. Cheese samples

217 without film and wrapped in PVC cling film were used as control.

218

219 **2.4.5. Statistical analysis**

220

221 All data were subjected to analysis of variance (ANOVA). Mean values were compared

222 using the Tukey's test at a confidence level of 95% ($p < 0.05$).

223

224 3. RESULTS AND DISCUSSION

225

226 **3.1. Functionalization of CNCs with rosin**

227

228 The surface functionalization of CNCs with rosin was confirmed by XPS (Fig. 1a-b) and

229 FTIR (Fig. 1c). The full XPS spectra of CNCs and r-CNCs show that the surfaces of both samples

230 contained mainly carbon and oxygen atoms (signals at 248 and 532 eV, respectively). The C1s

231 signal was deconvoluted to quantify the relative abundance of the carbon atom types, which

232 displayed 4 peaks attributed to C1 (C-C at 285.0 eV), C2 (C-O at 286.6 eV), C3 (O-C-O at 288.0

233 eV) and C4 (-O-C=O at 289.1 eV) [44]. The esterification of CNCs surface with rosin changed the

234 relative proportion of C4 and C1 peaks due to the higher amount of aliphatic carbon from rosin.

235 Furthermore, the O/C ratio decreased from 0.61 to 0.33 (Table 1), also confirming the successful

236 grafting of rosin onto the CNCs. Niu et al. [39] found similar behavior for rosin-modified cellulose

237 nanofibers. The chemical grafting of CNCs with rosin was analyzed by ATR-FTIR (Fig. 1c).

238 Typical vibration bands of cellulose were observed in the CNCs and r-CNCs spectra, including O-H

239 stretching at 3340 cm^{-1}, C-H symmetrical stretching at 2895 cm^{-1}, H-O-H bending of absorbed

240 water molecules at 1647 cm^{-1}, CH$_2$ symmetrical bending at 1427 cm^{-1}, and C-O-C vibration on

glycosidic linkages at 1165 cm^{-1} [37,39]. After chemical grafting, a new band at 1740 cm^{-1} was observed in the spectrum of r-CNCs, assigned to ester carbonyl groups from the reaction between the OH groups of CNCs and –COOH groups of rosin. Likewise, the increased intensity of the band at 1647 cm^{-1} can be related to C=C stretching from rosin cyclic alkene rings, which was also observed by PM-IRRAS. There was no significant reduction in the intensity of the OH band at 3340 cm^{-1}, indicating that esterification occurred mainly with hydroxyl groups accessible at the CNCs surface, as reported by Castro et al. [37]. The absence of a band at ~1700 cm^{-1} from rosin carbonyl groups indicates that the residual rosin was completely removed after the purification step. The TEM images of CNCs and r-CNCs in Fig. 1d-e show that the needle-like shape of the nanocrystals was unchanged after functionalization with rosin, as expected. The average lengths for CNCs and r-CNCs were 108.0 ± 33 and 122.0 ± 50 nm, and the average diameters were 3.8 ± 0.9 and 7.5 ± 2.2 nm, respectively. The largest dimensions of r-CNCs are attributed to the small aggregates of CNCs crystals. This is consistent with Espino-Pérez et al. [28] who observed the largest length for octadecyl isocyanate-grafted CNCs (179.0 nm) compared with non-grafted CNCs (155.0 nm). A schematic representation of the rosin-functionalized CNCs is shown in Fig. 1f.
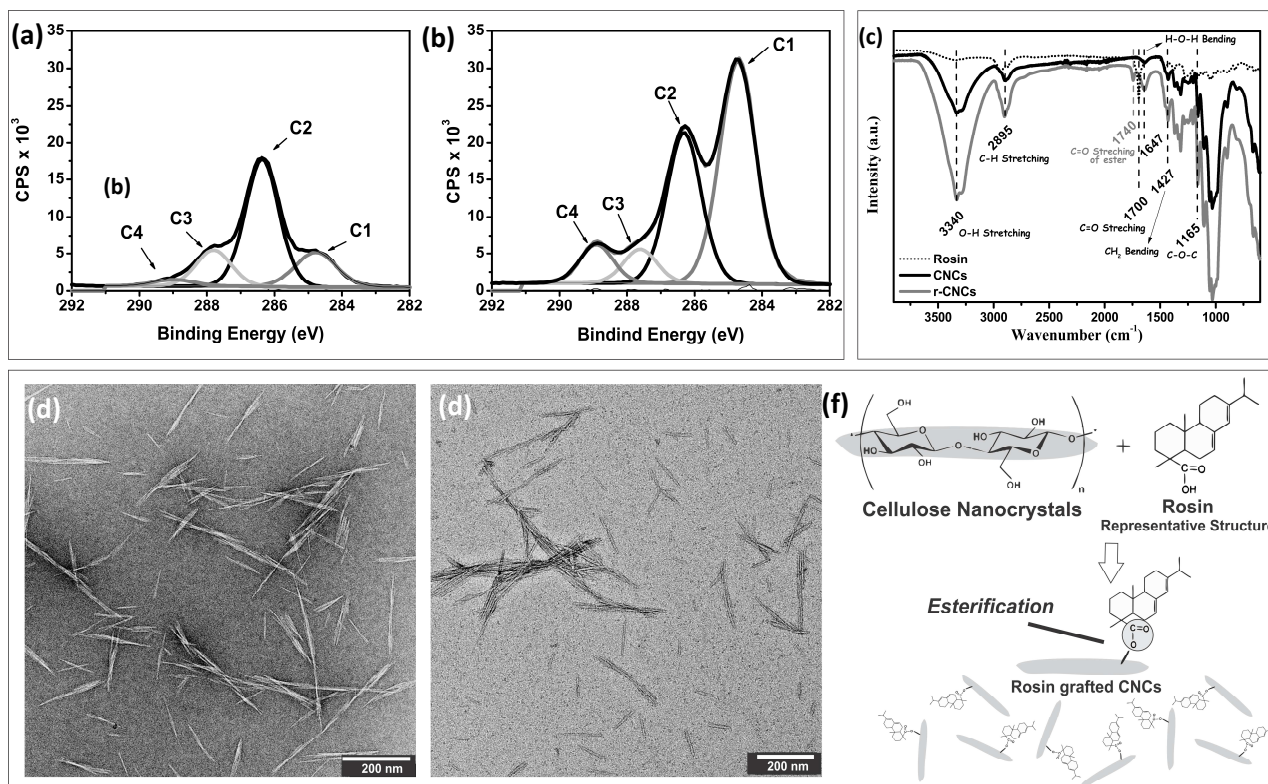
Table 1: X-ray photoelectron spectroscopy data of CNCs and r- CNCs

| Cellulose nanoparticles	O/C	Binding energy, eV			
		C1: C-C 285.0	C2: C-O 286.6	C3: O-C-O 288.0	C4: O=C-O 289.1
CNCs	0.61	16.4	62.6	17.2	3.8
r-CNCs	0.33	52.1	32.5	7.3	8.1

Fig. 1. C_{1s} XPS spectra of (a) CNCs and (b) r-CNCs. (c) ATR-FTIR spectra of rosin, CNCs, and r-CNCs. (d) TEM micrographs of CNCs and (e) r-CNCs. (f) schematic representation of rosin-functionalized CNCs.

The XRD patterns of CNCs and r-CNCs are displayed in Fig. S2 in the Supporting Information. Both samples exhibited typical diffraction peaks at $2\theta = 16.5$, 22.7, and 34.8°, related to cellulose I polymorph [37]. This confirms that rosin grafting did not convert cellulose I into cellulose II. The crystallinity index slightly increased from 82% to 84% after functionalization. Similar behavior was reported by Niu et al. [39], who found crystallinity indexes of 59.91 and 63.42% for CNF and rosin-CNF, respectively. These increases in crystallinity were attributed to the partial hydrolysis of the nanocellulose amorphous phase due to the acidic condition used in the reaction with rosin [39].

3.2. Morphology and optical properties of gelatin films reinforced with CNCs and r-CNCs

275   Pure gelatin and bionanocomposite films of different CNCs and r-CNCs contents were

276   obtained with solution casting. The thickness of the free-standing films was similar (~ 85 µm) for

277   all compositions with standard deviations lower than 20%. The dispersion of CNCs and r-CNCs in

278   the gelatin matrix was studied by SEM, as shown in Fig. 2. The gelatin films with low CNCs

279   content had smooth and more regular surfaces. The absence of agglomerates for the film with 4.0

280   wt% r-CNCs content is suggested from the SEM image in Fig. 2c, indicating a good dispersion of r-

281   CNCs [45] within the gelatin matrix. Nevertheless, agglomerates appeared when 6.0 wt% r-CNCs

282   were added to the gelatin film (Fig. 2e). This is probably due to the increased hydrophobicity of r-

283   CNCs after functionalization with rosin, which decreased chemical compatibility with the

284   hydrophilic gelatin matrix. The evidence of increased hydrophobicity in gelatin/r-CNCs films is

285   provided by contact angle measurements (Fig. S3 in the Supporting Information).

286
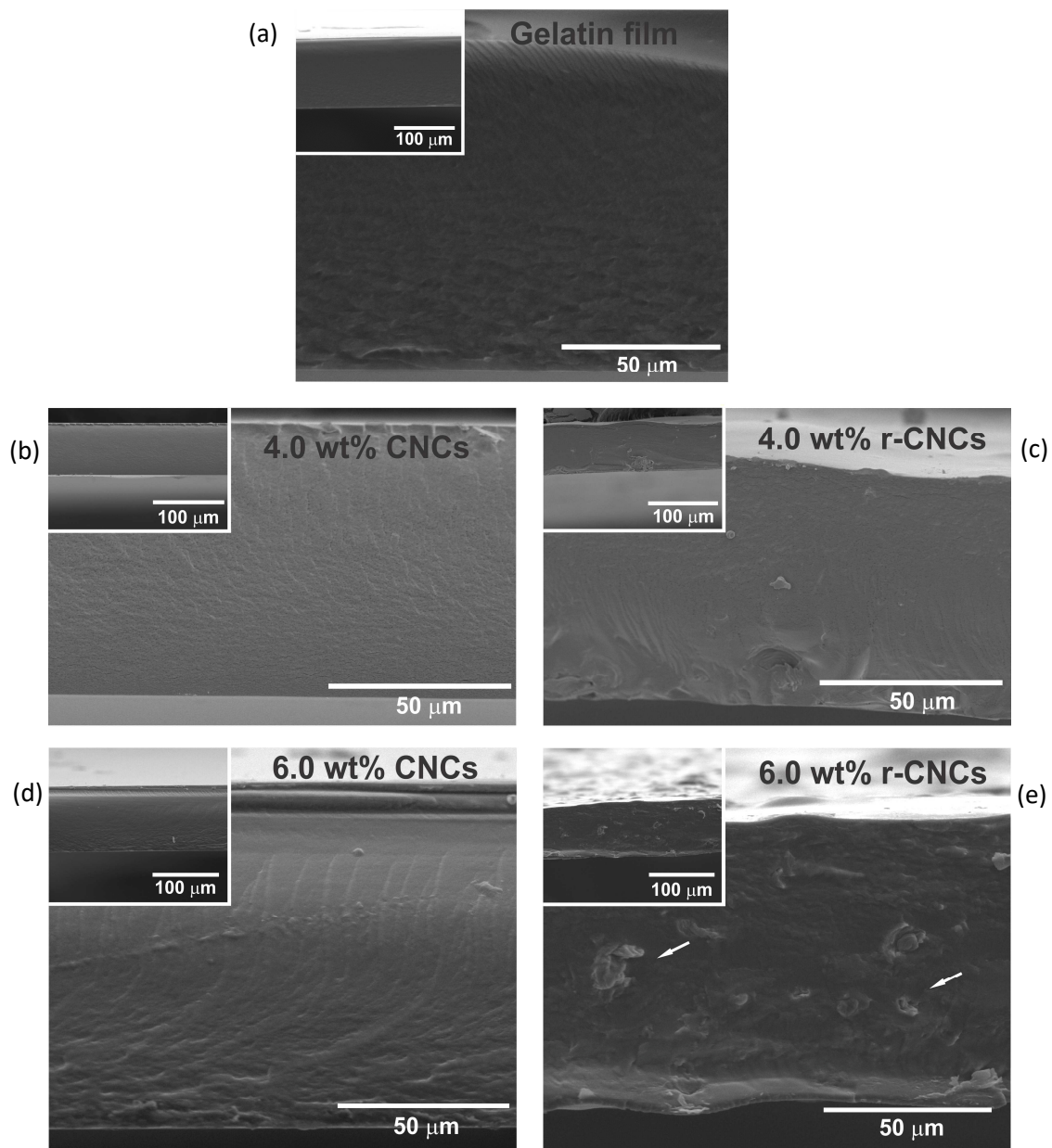
Fig. 2. SEM micrographs of the cross-sectional surface of (a) pure gelatin film and gelatin bionanocomposites with 4.0 wt% (b) CNCs and (c) r-CNCs, and with 6.0 wt% (d) CNCs and (e) r-CNCs content.

Polarization-modulated infrared reflection-absorption spectroscopy (PM-IRRAS) was performed to infer filler/matrix interactions in the CNCs- and r-CNCs-based gelatin bionanocomposites [46]. The PM-IRRAS signal has an overall dependence on the number of chemical group dipoles at the sample surface and on the orientation of these dipoles. Fig. 3 shows

296   representative PM-IRRAS spectra for the pure gelatin film and bionanocomposite films containing

297   6.0 wt% CNCs or r-CNCs. The bands and calculated areas are summarized in Table S1 and Fig. S4,

298   respectively, in the Supporting Information. For the pure gelatin film, the spectrum displays typical

299   bands of gelatin structure. The bands at 1388, 1523 and 1755/1760 cm^{-1} are ascribed to amide III,

300   amide II (60% N-H and 40% C-N) and C=O dipoles, respectively [47–49], while the band at 1625

301   cm^{-1} may be attributed to amide I (80% C=O, 10% N-H and 10% C-N). These bands also appeared

302   in the PM-IRRAS spectra of the bionanocomposites, but their areas were slightly reduced with the

303   addition of 6 wt% CNCs, most likely because of the total gelatin content in the film decreased from

304   83 to 79%. An opposite trend was observed for the 6 wt% r-CNCs-loaded gelatin

305   bionanocomposite, whose spectrum showed that the area/intensity of the amide bands increased,

306   suggesting dipole reorientation in the presence of r-CNCs. There was also a contribution of the C=C

307   dipoles from the rosin alkene rings on the amide I band intensity [47–49]. The spectral range

308   ascribed to C=O dipoles was also modified in the spectrum, with larger area reduction for the band

309   at 1755/1760 cm^{-1} than in the other samples. In addition, there was a new band at 1712 cm^{-1}, which

310   can be assigned to the ester carbonyl (C=O) groups from the r-CNCs, as already observed by ATR-

311   FTIR. The PM-IRRAS spectra reveal that the chemical environment of the dipole-forming gelatin

312   groups was more effectively disturbed with r-CNCs rather than with CNCs. This suggests that the

313   filler/matrix interactions in the gelatin/r-CNCs bionanocomposites encompass dipole-dipole

314   interactions in addition to hydrogen bonding, which is the only chemical interaction expected in the

315   case of CNCs.
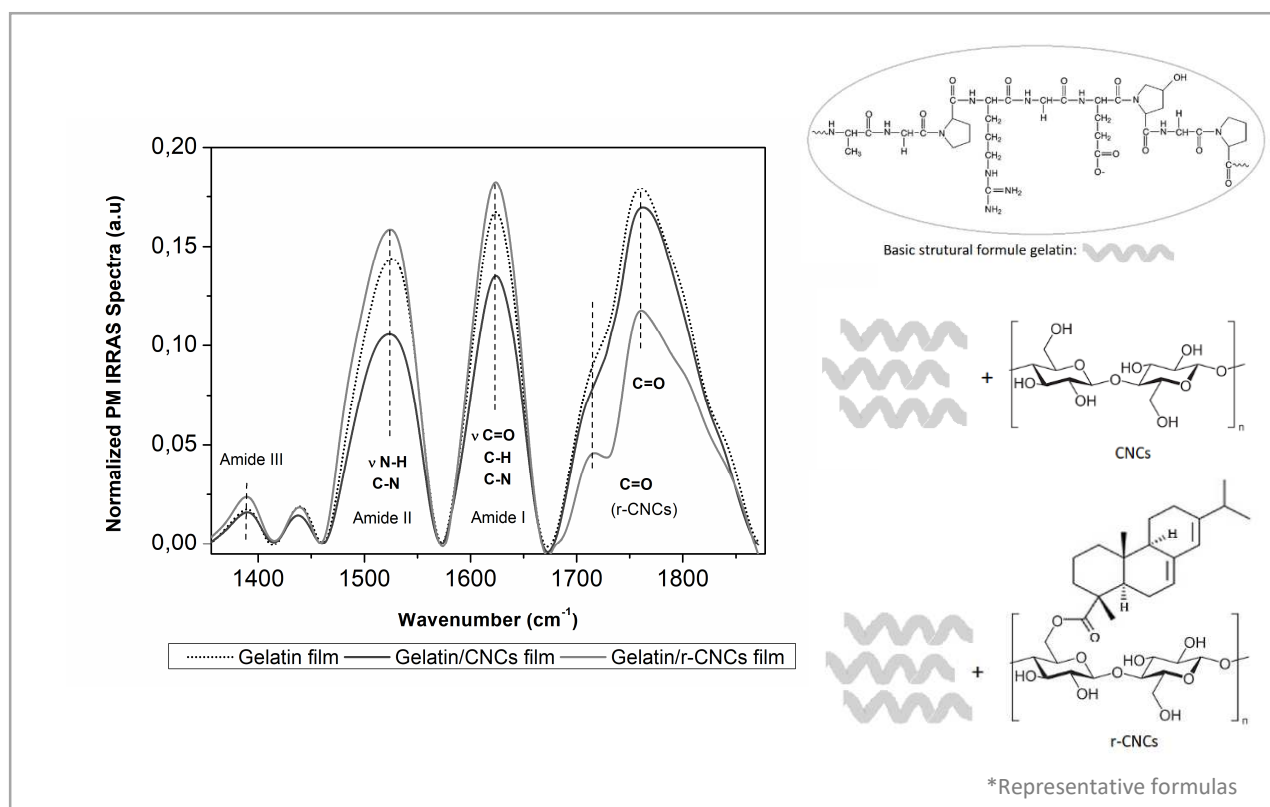
316

317

318

319

320

Fig. 3: PM-IRRAS spectra of gelatin film and gelatin bionanocomposites with 6 wt% CNCs and 6 wt% r-CNCs. The spectrum of a clean gold substrate was used as a baseline.

All gelatin/CNCs and gelatin/r-CNCs bionanocomposites were flexible, and exhibited good macroscopic homogeneity and high light transparency, as displayed in Fig. 4 and in the UV-Vis transmittance spectra in Fig. S5 in the Supporting Information. The gelatin film exhibited a high barrier against UV radiation, nearly 100% for UVC, over 93.3% for UVB, and 54.0% for UVA, due to chromophore groups such as tyrosine and phenylalanine [50]. The addition of r-CNCs led to a significant reduction in the transmittance over all the UV range compared to the neat gelatin and gelatin/CNCs film samples. The gelatin film with 0.5 wt% r-CNCs showed a reduction of 20.8 and 29.1 % in the UVB and UVA transmittance, respectively, compared to the gelatin/CNCs films. Narayanan et al. [36] observed a reduction of 1% and 6% for UVB and UVA, respectively, in PLA bionanocomposites with 20 wt% rosin. The authors attributed this behavior to the absorption properties of rosin, which prevented light transmission through the films. However, the gelatin film

with 6.0 wt% r-CNCs showed a significant reduction in the visible light range, which indicates light scattering by r-CNCs aggregates, as shown in the SEM images (Fig. 2e). Table 2 presents a comparison of light transmission between the gelatin/r-CNCs bionanocomposites and some synthetic packaging films. The gelatin/r-CNCs films had low transmittance over the entire spectral range, indicating that they absorbed light much more efficiently than several synthetic polymer films. These results suggest that the gelatin/r-CNCs bionanocomposites are suitable as packaging to protect light-sensitive food products.
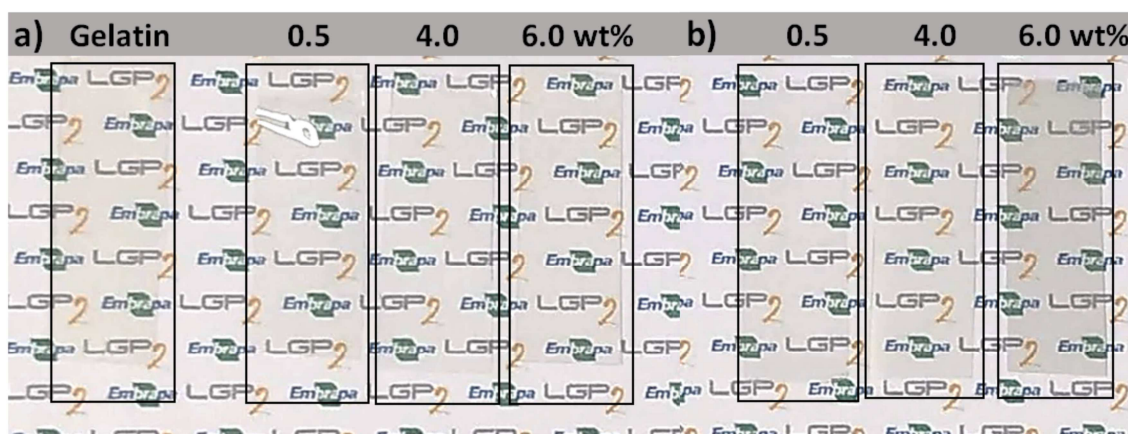
Fig. 4. Photography of (a) gelatin/CNCs and (b) gelatin/r-CNCs bionanocomposite films

Table 2: Optical properties of gelatin/r-CNCs bionanocomposites and synthetic packaging films.

Film	Light transmission (%)			
	200 nm	280 nm	400 nm	600 nm
0.5 wt% gelatin/r-CNCs	0.0	4.5	77.3	87.4
6.0 wt% gelatin/r-CNCs	0.0	5.4	60.5	66.7
Synthetic films currently applied in food packaging [a]				
LDPE[a]	13.1	67.5	83.4	86.9
OPP[a]	4.6	80.0	87.9	89.1
PVC	20	83.9	87.9	88.7

LDPE: low-density polyethylene; OPP: oriented polypropylene; PVC: poly(vinyl chloride)
[a] adapted from [51].

3.3. Barrier and mechanical properties of gelatin/CNCs and gelatin/r-CNCs films

Water vapor permeability (WVP) and oxygen transmission rate (OTR) are barrier properties that determine the ability of bio-based films to protect food products from moisture and O_2 transfer, lipid oxidation, and loss of volatile aromas and flavors. Gelatin films generally display good barrier against oxygen at low and intermediate relative humidity [52]. Our results show that the OTR of the gelatin films with 0.5 and 6.0 wt% CNCs and r-CNCs at 0% and 80% RH were < 0.01 cm³/m².day, indicating that the addition of CNCs or r-CNCs did not change significantly the already high oxygen barrier of gelatin. The values of WVP and WVTR of the gelatin bionanocomposites with CNCs and r-CNCs at 25 ˚C and 50% RH are presented in Fig. S6 in the Supporting Information. The pure gelatin film exhibited a WVP of 0.20 ± 0.03 g mm/m^2 h kPa. The incorporation of CNCs or r-CNCs reduced the WVP of the gelatin films. The addition of 0.5 wt% r-CNCs significantly decreased the WVP by 55% ($p < 0.05$). According to Ooi, Ahmad, & Amin [53], nanoparticles can reduce WVP by increasing the biopolymer crystallinity or by reducing the free hydrophilic groups (OH, NH) in the gelatin matrix, thereby creating a tortuous pass for water vapor diffusion through the film matrix. Santos et al. [54] reported decreased WVP of protein films with increasing CNCs content. They found that fish gelatin films with 15 wt% CNCs had WVP values of approximately 2 g mm/m^2 h kPa (25 ˚C at 85% RH). George & Siddaramaiah [24] reported that 4.0 wt% bacterial cellulose nanocrystals reduced WVP of gelatin, and attributed this outcome to the low hygroscopicity of highly crystalline CNCs. They found WVP values of around 0.175 g mm/m^2 h kPa (25 ˚C at 50% RH), which were higher than those of our gelatin films reinforced with CNCs or r-CNCs.

The mechanical properties (Young's modulus, tensile strength, and elongation at break) of the bionanocomposite films were investigated with tensile tests. The Young's modulus and tensile strength of the pure gelatin film were 743 and 17 MPa, respectively, as shown in Fig. 5. For gelatin/CNCs bionanocomposite films, the tensile strength and Young's modulus increased

significantly with increasing the CNCs content. This can be attributed to the effective CNCs reinforcing effect through stress transfer from the gelatin matrix to CNCs [21]. For the same filler content of 4.0 wt%, the gelatin film with r-CNCs exhibited tensile strength ~30% higher than that of the film with CNCs. This improvement is likely due to van der Waals forces (e.g. dipole-dipole interactions) and hydrogen bonds between the r-CNCs and gelatin matrix. However, for gelatin/r-CNCs film with 6.0 wt% r-CNCs, a reduction in Young's modulus and tensile strength was observed. In addition, there was an increase in elongation at break, which can be attributed to the formation of agglomerates, as revealed by SEM. The gelatin film with 6.0 wt% r-CNCs showed an elongation at break ~145% higher than that of the pure gelatin film, indicating that the gelatin/r-CNCs films were much more ductile and flexible. The interaction formed between the gelatin and r-CNCs weakened the protein-protein interactions, which were effective in stabilizing the gelatin network, as described by Zhuang et al [22]. Therefore, it is clear that r-CNCs play an effective role in enhancing the mechanical properties of gelatin, with promising features for flexible food packaging.
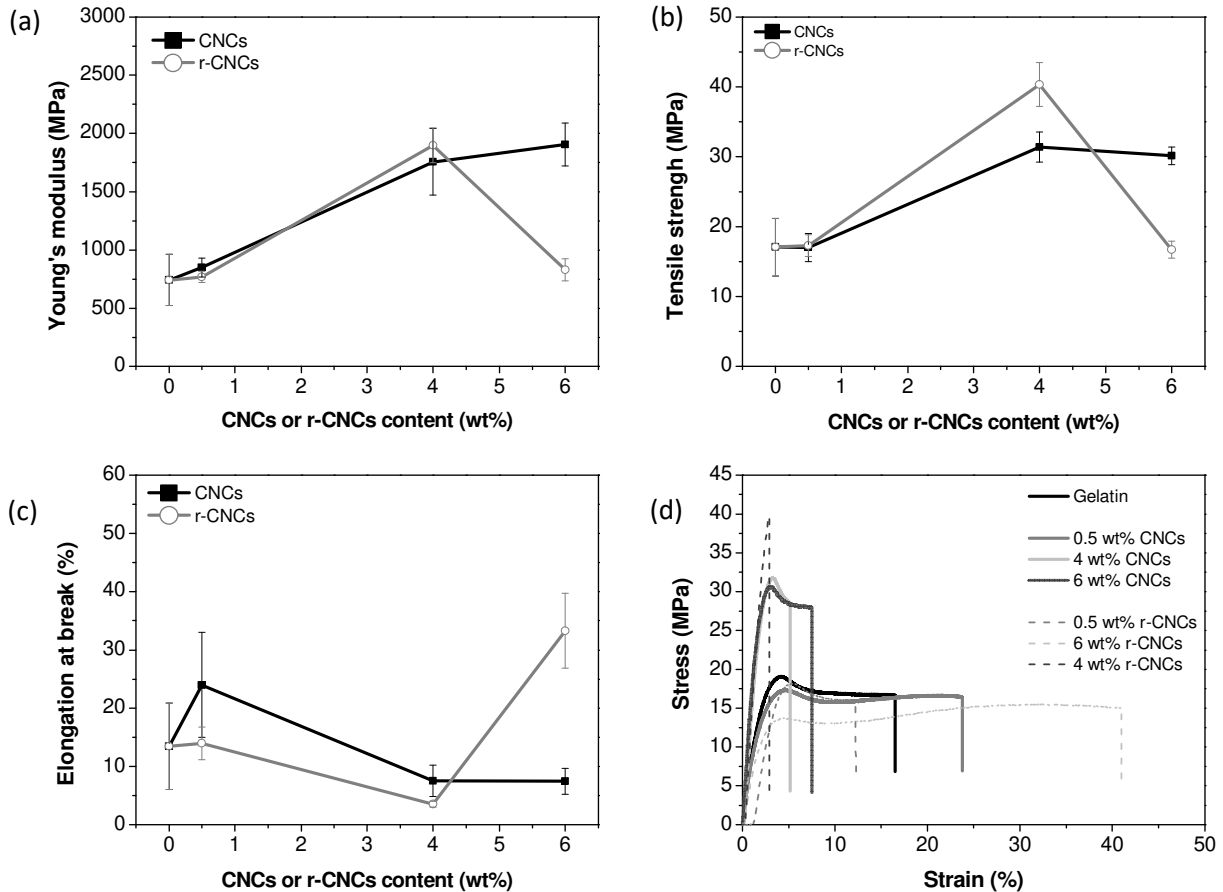
Fig. 5. (a) Young's modulus, (b) tensile strength (c) elongation at break, and (d) stress-strain curves as a function of CNCs and r-CNCs content in bionanocomposite gelatin films obtained by casting.
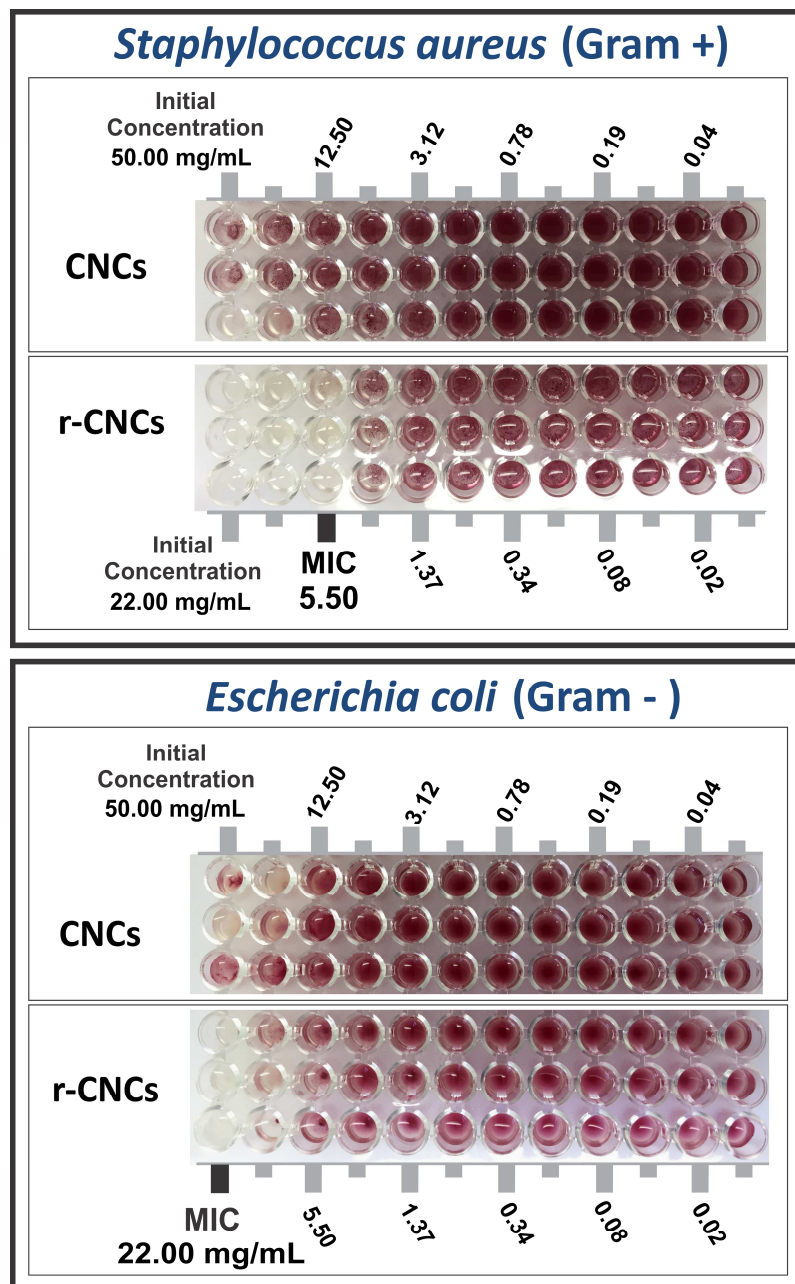
3.4. Antimicrobial properties of r-CNCs and gelatin/r-CNCs films

The minimum inhibitory concentration (MIC) value was determined as the lowest concentration of r-CNCs suspension that inhibited the growth of the tested microorganisms. The results in Fig. 6 show the highest bactericidal effect against Gram-positive *Staphylococcus aureus* and Gram-negative *Escherichia coli* with the r-CNCs suspension. As expected, there was no inhibitory effect for the CNCs suspension. A low concentration of r-CNCs (5.5 mg/mL) inhibited the growth of *S. aureus*, whereas for *E coli* inhibition a concentration of 22 mg/mL was required. This may be due to the external lipopolysaccharide layer of the cell membrane of Gram-negative
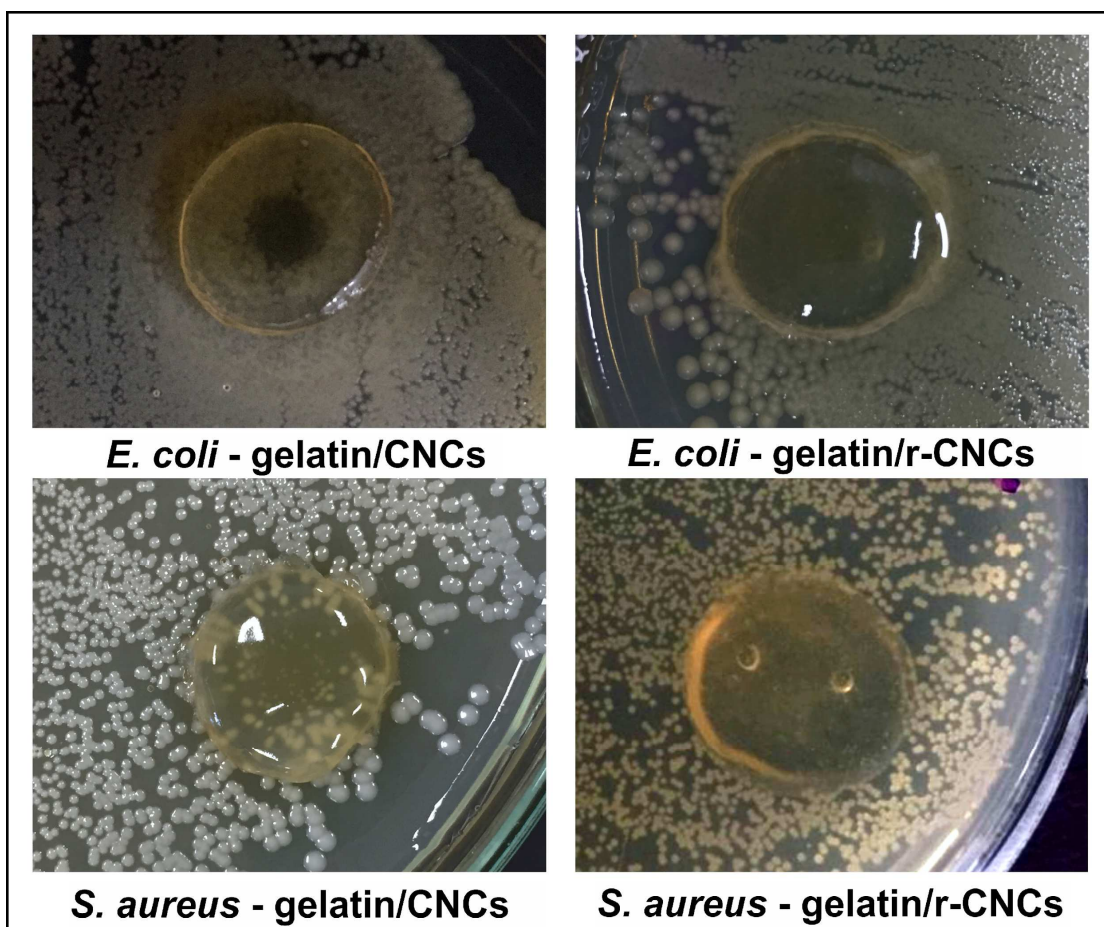
bacteria, which restricts diffusion of hydrophobic compounds [55]. The proposed mechanism for the r-CNCs antimicrobial activity is based on its interaction with the phospholipid cell membrane, which causes increased permeability and leakage of cytoplasm, or its reaction with enzymes located at the cell wall [56]. This is consistent with findings that rosin-derived cationic compounds have antimicrobial activity against many bacteria due to the hydrophobicity and structure of resin acids [57].

418   Fig. 6. Minimum inhibitory concentration (MIC) of CNCs and r-CNCs suspension tested on

419   Gram-positive *Staphylococcus aureus* and Gram-negative *Escherichia coli.*

420   The gelatin/r-CNCs films were also tested against *S. aureus* and *E. coli* as demonstrated by

421   the agar diffusion assays depicted in Fig. 7. The control films made with CNCs in gelatin did not

422   display any inhibitory effect, with bacteria observed underneath. On the other hand, the gelatin/r-

423   CNCs films showed an effective antibacterial property, especially against *E. coli,* since there was no

424   bacterial growth in the inhibition area covered with the films. Neither of the tested films yielded a

425   halo or a surrounding clearing zone, which shows that r-CNCs do not diffuse through the adjacent

426   agar media and their antimicrobial effect is likely to occur by contact. The lack of diffusion is

427   related to the hydrophobic nature of rosin molecules grafted onto the r-CNCs. Indeed, migration is

428   linked to factors such as molecule size, polarity, shape, and quantity of water in the agar, in addition

429   to the chemical structure and crosslinking in the films [58].


430

E. coli - gelatin/CNCs   *E. coli* - gelatin/r-CNCs

S. aureus - gelatin/CNCs   *S. aureus* - gelatin/r-CNCs

431   Fig. 7. Agar overlay assay of gelatin film discs against *S. aureus* and *E .coli*.

3.5. Use of gelatin films reinforced with r-CNCs as packaging materials

        Accelerated storage tests were carried out at 25 ºC for one month to prove the antimicrobial ability of gelatin/r-CNCs films in practical applications. The tests were conducted with mozzarella cheese samples packed with pure gelatin, 6 wt% r-CNCs gelatin film, and a PVC film. Mozzarella cheese is perishable and suffers either from fungal or bacterial spoilage depending on the storage conditions. Fig. 8 shows evident microbial spoilage in the control and gelatin-packed cheese samples, and especially in the sample packed in PVC. In contrast, there was no microbial growth in the sample packed in 6 wt% r-CNCs-loaded gelatin film. As a proof of concept, we illustrated that the gelatin/r-CNCs bionanocomposite films can extend the shelf-life of mozzarella cheese, also providing a direct indication of the antibacterial activity of r-CNCs even after forming nanocomposites with gelatin. However, it is possible that r-CNCs migrated towards the oily cheese surface in contact with the film, but this has to be confirmed with further quantitative studies.
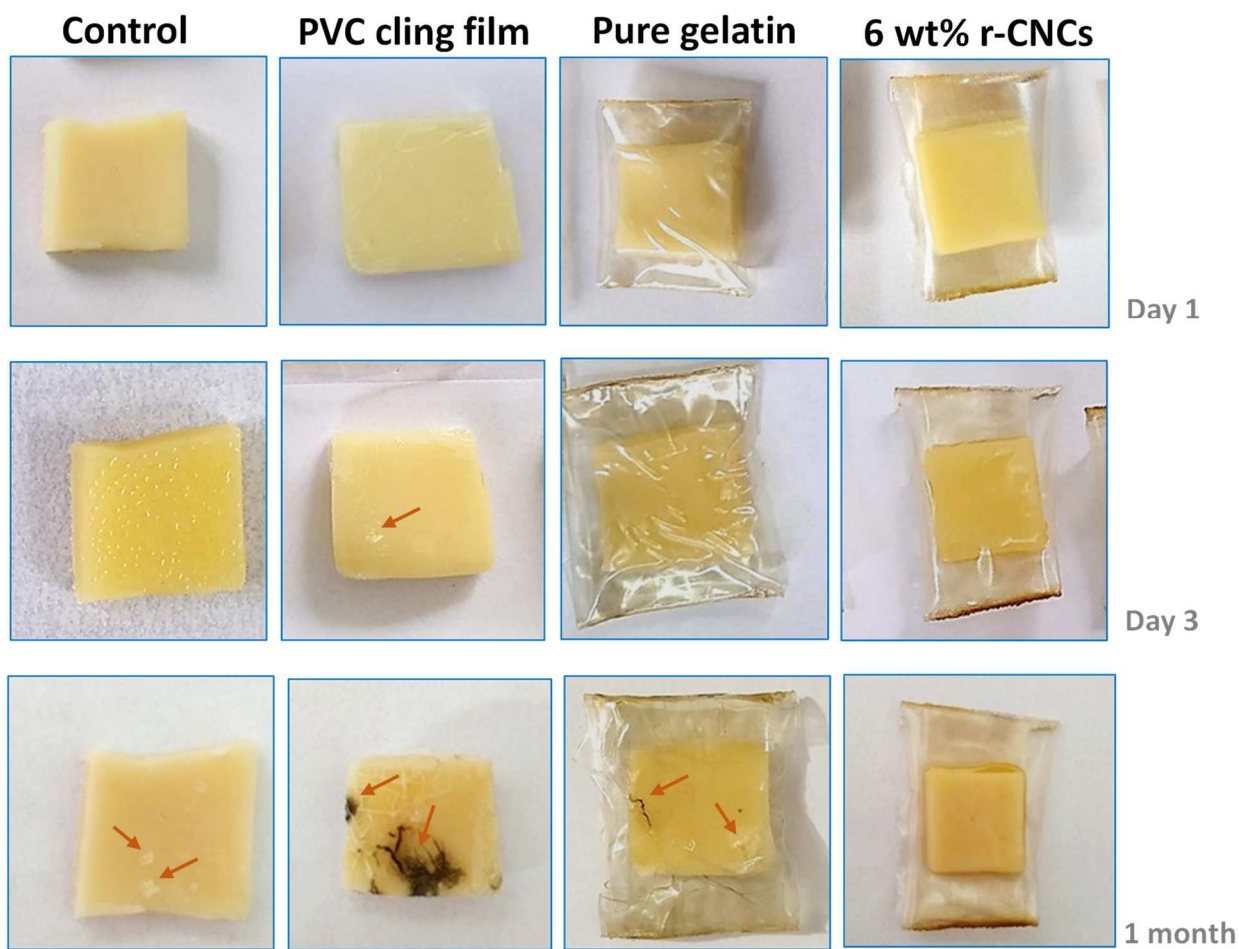
Fig. 8: Schematic comparison of accelerated storage for mozzarella cheese slices packed in a PVC cling film, pure gelatin film, and gelatin/r-CNCs nanocomposite (6 wt%) film over 30 days at 25 ℃. The control refers to free-standing, unpacked cheese slices (The Brazilian version of mozzarella cheese can be sliced, in contrast to the Italian mozzarella). Microbial spoilage is indicated by arrows in the images.

4. CONCLUSION

CNCs were successfully functionalized with rosin and used as a bactericidal nanofiller in gelatin for achieving multifunctional packaging. In particular, the r-CNCs consistently improved the optical, and water vapor barrier properties of gelatin films as compared to conventional CNCs. The mechanical strength of the gelatin matrix was increased and could be tuned by varying the r-CNCs

content. This study demonstrates how grafting reactions can extend the functionalities of nanocelluloses for use in flexible packaging materials, which otherwise would suffer from limited physical and biological properties. The results from microbial assays confirmed the potential of gelatin/r-CNCs nanocomposites in increasing the shelf-life of cheese samples. We expect that these findings will serve as a basis for future design of new functionalized nanocellulose/gelatin films for food storage under various conditions.

AUTHOR INFORMATION

Corresponding Author

*E-mail: Julien.Bras@rd.nestle.com. Address: Nestle Research Center, 57 route du Jorat 1010, Lausanne, Switzerland. Phone: +33 7 86 05 24 45.

ORCID

Julien Bras: 0000-0002-2023-5435

Author Contributions

The manuscript was written through contributions of all authors. All authors have given approval to the final version of the manuscript.

Notes

The authors declare no competing financial interest.

489

490 ABBREVIATIONS

491 CNCs Cellulose nanocrystals, r-CNCs cellulose nanocrystals functionalized with rosin

492 REFERENCES

493

494 [1]   N.A. Al-Tayyar, A.M. Youssef, R. Al-hindi, Antimicrobial food packaging based on

495   sustainable Bio-based materials for reducing foodborne Pathogens: A review, Food Chem.

496   310 (2020) 125915. https://doi.org/10.1016/j.foodchem.2019.125915.

497 [2]   S. Shankar, X. Teng, G. Li, J. Rhim, Preparation, characterization, and antimicrobial activity

498   of gelatin/ZnO nanocomposite films, Food Hydrocoll. 45 (2015) 264–271.

499   https://doi.org/10.1016/j.foodhyd.2014.12.001.

500 [3]   F. Garavand, M. Rouhi, S.H. Razavi, I. Cacciotti, R. Mohammadi, Improving the integrity of

501   natural biopolymer films used in food packaging by crosslinking approach: A review, Int. J.

502   Biol. Macromol. 104 (2017) 687–707. https://doi.org/10.1016/j.ijbiomac.2017.06.093.

503 [4]   B. Hassan, S.A.S. Chatha, A.I. Hussain, K.M. Zia, N. Akhtar, Recent advances on

504   polysaccharides, lipids and protein based edible films and coatings: A review, Int. J. Biol.

505   Macromol. 109 (2018) 1095–1107. https://doi.org/10.1016/j.ijbiomac.2017.11.097.

506 [5]   S. Sivakanthan, S. Rajendran, A. Gamage, T. Madhujith, S. Mani, Antioxidant and

507   antimicrobial applications of biopolymers: A review, Food Res. Int. 136 (2020).

508   https://doi.org/10.1016/j.foodres.2020.109327.

509   [6]   J. Gómez-Estaca, C. López-de-Dicastillo, P. Hernández-Muñoz, R. Catalá, R. Gavara,

510   Advances in antioxidant active food packaging, Trends Food Sci. Technol. 35 (2014) 42–51.

511   https://doi.org/10.1016/j.tifs.2013.10.008.

512   [7]   J.W. Han, L. Ruiz-Garcia, J.P. Qian, X.T. Yang, Food Packaging: A Comprehensive Review

513   and Future Trends, Compr. Rev. Food Sci. Food Saf. 17 (2018) 860–877.

514   https://doi.org/10.1111/1541-4337.12343.

515   [8]   J. Wang, J. Fang, L. Wei, Y. Zhang, H. Deng, Y. Guo, C. Hu, Y. Meng, Decrease of

516   microbial community diversity, biogenic amines formation, and lipid oxidation by phloretin

517   in Atlantic salmon fillets, Lwt. 101 (2019) 419–426.

518   https://doi.org/10.1016/j.lwt.2018.11.039.

519   [9]   H. Moustafa, A.M. Youssef, N.A. Darwish, A.I. Abou-Kandil, Eco-friendly polymer

520   composites for green packaging: Future vision and challenges, Compos. Part B Eng. 172

521   (2019) 16–25. https://doi.org/10.1016/j.compositesb.2019.05.048.

522   [10]   S. Esteghlal, M. Niakousari, S.M.H. Hosseini, Physical and mechanical properties of gelatin-

523   CMC composite films under the influence of electrostatic interactions, Int. J. Biol.

524   Macromol. 114 (2018) 1–9. https://doi.org/10.1016/j.ijbiomac.2018.03.079.

525   [11]   X. Liu, Z. Ji, W. Peng, M. Chen, L. Yu, F. Zhu, Chemical mapping analysis of compatibility

526   in gelatin and hydroxypropyl methylcellulose blend films, Food Hydrocoll. 104 (2020)

527   105734. https://doi.org/10.1016/j.foodhyd.2020.105734.

528   [12]   Z. Wang, J. Zhou, X. xuan Wang, N. Zhang, X. xiu Sun, Z. su Ma, The effects of

529   ultrasonic/microwave assisted treatment on the water vapor barrier properties of soybean

530   protein isolate-based oleic acid/stearic acid blend edible films, Food Hydrocoll. 35 (2014)

531   51–58. https://doi.org/10.1016/j.foodhyd.2013.07.006.

532   [13]   M.C. Gómez-Guillén, M. Pérez-Mateos, J. Gómez-Estaca, E. López-Caballero, B. Giménez,

533   P. Montero, Fish gelatin: a renewable material for developing active biodegradable films,

534   Trends Food Sci. Technol. 20 (2009) 3–16. https://doi.org/10.1016/j.tifs.2008.10.002.

535   [14] H.M.C. Azeredo, M.F. Rosa, L.H.C. Mattoso, Nanocellulose in bio-based food packaging

536   applications, Ind. Crops Prod. 97 (2017) 664–671.

537   https://doi.org/10.1016/j.indcrop.2016.03.013.

538   [15] G. Siqueira, J. Bras, A. Dufresne, Cellulosic Bionanocomposites: A Review of Preparation,

539   Properties and Applications, Polymers (Basel). 2 (2010) 728–765.

540   https://doi.org/10.3390/polym2040728.

541   [16] S.F. Hosseini, M.C. Gómez-Guillén, A state-of-the-art review on the elaboration of fish

542   gelatin as bioactive packaging: Special emphasis on nanotechnology-based approaches,

543   Trends Food Sci. Technol. 79 (2018) 125–135. https://doi.org/10.1016/j.tifs.2018.07.022.

544   [17] H.M.C. de Azeredo, Nanocomposites for food packaging applications, Food Res. Int. 42

545   (2009) 1240–1253. https://doi.org/10.1016/j.foodres.2009.03.019.

546   [18] P. Squinca, S. Bilatto, A.C. Badino, C.S. Farinas, Nanocellulose production in future

547   biorefineries: an integrated approach using tailor-made enzymes Nanocellulose production in

548   future biorefineries : an integrated approach using tailor-made enzymes, ACS Sustain. Chem.

549   Eng. 8 (2020) 2277–2286. https://doi.org/10.1021/acssuschemeng.9b06790.

550   [19] B. Thomas, M.C. Raj, K.B. Athira, M.H. Rubiyah, J. Joy, A. Moores, G.L. Drisko,

551   Nanocellulose, a versatile green platform: from biosources to materials and their

552   applications, Chem. Rev. 118 (2018) 11575–11625.

553   https://doi.org/10.1021/acs.chemrev.7b00627.

554   [20] R.J. Moon, G.T. Schueneman, J. Simonsen, Overview of Cellulose Nanomaterials, Their

555   Capabilities and Applications, Jom. 68 (2016) 2383–2394. https://doi.org/10.1007/s11837-

556   016-2018-7.

557   [21] A. Dufresne, Polysaccharide nanocrystal reinforced nanocomposites, Can. J. Chem. 86

558   (2008) 484–494. https://doi.org/10.1139/V07-152.

559   [22]   C. Zhuang, F. Tao, Y. Cui, Eco-friendly biorefractory films of gelatin and TEMPO-oxidized

560   cellulose ester for food packaging application, J. Sci. Food Agric. 97 (2017) 3384–3395.

561   https://doi.org/10.1002/jsfa.8189.

562   [23]   P. Sukyai, P. Anongjanya, N. Bunyahwuthakul, K. Kongsin, N. Harnkarnsujarit, U. Sukatta,

563   R. Sothornvit, R. Chollakup, Effect of cellulose nanocrystals from sugarcane bagasse on

564   whey protein isolate-based films, Food Res. Int. 107 (2018) 528–535.

565   https://doi.org/10.1016/j.foodres.2018.02.052.

566   [24]   J. George, Siddaramaiah, High performance edible nanocomposite films containing bacterial

567   cellulose nanocrystals, Carbohydr. Polym. 87 (2012) 2031–2037.

568   https://doi.org/10.1016/j.carbpol.2011.10.019.

569   [25]   L.S.F. Leite, C.M. Ferreira, A.C. Corrêa, F.K.V. Moreira, L.H.C. Mattoso, Scaled-up

570   production of gelatin-cellulose nanocrystal bionanocomposite films by continuous casting,

571   Carbohydr. Polym. 238 (2020) 116198. https://doi.org/10.1016/j.carbpol.2020.116198.

572   [26]   M. Le Gars, J. Bras, H. Salmi-Mani, M. Ji, D. Dragoe, H. Faraj, S. Domenek, N. Belgacem,

573   P. Roger, Polymerization of glycidyl methacrylate from the surface of cellulose nanocrystals

574   for the elaboration of PLA-based nanocomposites, Carbohydr. Polym. 234 (2020) 115899.

575   https://doi.org/10.1016/j.carbpol.2020.115899.

576   [27]   J. Tang, J. Sisler, N. Grishkewich, K.C. Tam, Functionalization of cellulose nanocrystals for

577   advanced applications, J. Colloid Interface Sci. 494 (2017) 397–409.

578   https://doi.org/10.1016/j.jcis.2017.01.077.

579   [28]   E. Espino-Pérez, J. Bras, G. Almeida, P. Relkin, N. Belgacem, C. Plessis, S. Domenek,

580   Cellulose nanocrystal surface functionalization for the controlled sorption of water and

581   organic vapours, Cellulose. 23 (2016) 2955–2970. https://doi.org/10.1007/s10570-016-0994-

582   y.

583   [29]   H.W. Kwak, H. Lee, S. Park, M.E. Lee, H.-J. Jin, Chemical and physical reinforcement of

584   hydrophilic gelatin film with di-aldehyde nanocellulose, Int. J. Biol. Macromol. 146 (2020)

585   332–342. https://doi.org/10.1016/j.ijbiomac.2019.12.254.

586 [30] N.A. El-Wakil, E.A. Hassan, R.E. Abou-Zeid, A. Dufresne, Development of wheat

587   gluten/nanocellulose/titanium dioxide nanocomposites for active food packaging, Carbohydr.

588   Polym. 124 (2015) 337–346. https://doi.org/10.1016/j.carbpol.2015.01.076.

589 [31] F. V. Ferreira, M. Mariano, I.F. Pinheiro, E.M. Cazalini, D.H.S. Souza, L.S.S. Lepesqueur,

590   C.Y. Koga-Ito, R.F. Gouveia, L.M.F. Lona, Cellulose nanocrystal-based poly(butylene

591   adipate-co-terephthalate) nanocomposites covered with antimicrobial silver thin films,

592   Polym. Eng. Sci. 59 (2019) pen.25066. https://doi.org/10.1002/pen.25066.

593 [32] R. Sharma, S.M. Jafari, S. Sharma, Antimicrobial bio-nanocomposites and their potential

594   applications in food packaging, Food Control. 112 (2020) 107086.

595   https://doi.org/10.1016/j.foodcont.2020.107086.

596 [33] Y. Zheng, K. Yao, J. Lee, D. Chandler, J. Wang, C. Wang, F. Chu, Well-defined renewable

597   polymers derived from gum rosin, Macromol. Commun. to Ed. 43 (2010) 5922–5924.

598   https://doi.org/10.1021/ma101071p.

599 [34] S. Kugler, P. Ossowicz, K. Malarczyk-Matusiak, E. Wierzbicka, Advances in rosin-based

600   chemicals: The latest recipes, applications and future trends, Molecules. 24 (2019) 1651–

601   1703. https://doi.org/10.3390/molecules24091651.

602 [35] X. Liu, W. Xin, J. Zhang, Rosin-based acid anhydrides as alternatives to petrochemical

603   curing agents, Green Chem. 11 (2009) 1018–1025. https://doi.org/10.1039/b903955d.

604 [36] M. Narayanan, S. Loganathan, R.B. Valapa, S. Thomas, T.O. Varghese, UV protective

605   poly(lactic acid)/rosin films for sustainable packaging, Int. J. Biol. Macromol. 99 (2017) 37–

606   45. https://doi.org/10.1016/j.ijbiomac.2017.01.152.

607 [37] D.O. de Castro, J. Bras, A. Gandini, N. Belgacem, Surface grafting of cellulose nanocrystals

608   with natural antimicrobial rosin mixture using a green process, Carbohydr. Polym. 137

609   (2016) 1–8. https://doi.org/10.1016/j.carbpol.2015.09.101.

610   [38] F. Li, S.Y.H. Abdalkarim, H. Yu, J. Zhu, Y. Zhou, Y. Guan, Bifunctional Reinforcement of

611   Green Biopolymer Packaging Nanocomposites with Natural Cellulose Nanocrystal–Rosin

612   Hybrids, ACS Appl. Bio Mater. 3 (2020) 1944–1954.

613   https://doi.org/10.1021/acsabm.9b01100.

614   [39] X. Niu, Y. Liu, Y. Song, J. Han, H. Pan, Rosin modified cellulose nanofiber as a reinforcing

615   and co-antimicrobial agents in polylactic acid/chitosan composite film for food packaging,

616   Carbohydr. Polym. 183 (2018) 102–109. https://doi.org/10.1016/j.carbpol.2017.11.079.

617   [40] E. Espino-Pérez, S. Domenek, N. Belgacem, C. Sillard, J. Bras, Green Process for Chemical

618   Functionalization of Nanocellulose with Carboxylic Acids, Biomacromolecules. 15 (2014)

619   4551–4560. https://doi.org/10.1021/bm5013458.

620   [41] L. Segal, J.J. Creely, A.E. Martin, M. Conrad, An Empirical Method for Estimating the

621   Degree of Crystallinity of Native Cellulose Using the X-Ray Diffractometer, Text. Res. J. 29

622   (1959) 786–794.

623   [42] N. Paudyal, V. Anihouvi, J. Hounhouigan, M. Ignatius, B. Sekwati-monang, W. Amoa-awua,

624   A. Atter, N. Bernice, S. Mbugua, A. Asagbra, W. Abdelgadir, J. Nakavuma, M. Jakobsen, W.

625   Fang, Microbiology prevalence of foodborne pathogens in food from selected African

626   countries – a meta-analysis, Int. J. Food Microbiol. 249 (2017) 35–43.

627   https://doi.org/10.1016/j.ijfoodmicro.2017.03.002.

628   [43] C. Ferrario, G. Andrea, M. Cristina, F. Turroni, C. Milani, S. Duranti, L. Mancabelli, M.

629   Mangifesta, G. Alessandri, D. Van Sinderen, M. Ventura, Microbiology next generation

630   sequencing-based multigene panel for high throughput detection of food-borne pathogens,

631   Int. J. Food Microbiol. 256 (2017) 20–29. https://doi.org/10.1016/j.ijfoodmicro.2017.05.001.

632   [44] E. hadji B. Ly, J. Bras, P. Sadocco, M.N. Belgacem, A. Dufresne, W. Thielemans, Surface

633   functionalization of cellulose by grafting oligoether chains, Mater. Chem. Phys. 120 (2010)

634   438–445. https://doi.org/10.1016/j.matchemphys.2009.11.032.

635   [45]   L.S.F. Leite, L.C. Battirola, L.C.E. da Silva, M. do C. Gonçalves, Morphological

636   investigation of cellulose acetate/cellulose nanocrystal composites obtained by melt

637   extrusion, J. Appl. Polym. Sci. 133 (2016) 1–10. https://doi.org/10.1002/app.44201.

638   [46]   R.F. Vázquez, M.A. Daza Millone, F.J. Pavinatto, V.S. Herlax, L.S. Bakás, O.N. Oliveira,

639   M.E. Vela, S.M. Maté, Interaction of acylated and unacylated forms of E. coli alpha-

640   hemolysin with lipid monolayers: a PM-IRRAS study, Colloids Surfaces B Biointerfaces.

641   158 (2017) 76–83. https://doi.org/10.1016/j.colsurfb.2017.06.020.

642   [47]   F. Severcan, P.I. Haris, Vibrational Spectroscopy in Diagnosis and Screening, 1 edition, IOS

643   Press, Amsterdam, 2012.

644   [48]   B. Więckowski, A., Korzeniewski, C., Braunschweig, Vibrational spectroscopy at electrified

645   interfaces, John Wiley & Sons, Inc., Hoboken, NJ, USA, 2013.

646   https://doi.org/10.1002/9781118658871.

647   [49]   N.B. Coltrup, L.H. Daly, S.E. Wiberley, Introduction to infrared and raman spectroscopy, 3rd

648   editio, Elsevier, Boston, 1990. https://doi.org/10.1016/B978-0-12-182552-2.X5001-3.

649   [50]   K. Chuaynukul, M. Nagarajan, T. Prodpran, S. Benjakul, P. Songtipya, L. Songtipya,

650   Comparative Characterization of Bovine and Fish Gelatin Films Fabricated by Compression

651   Molding and Solution Casting Methods, J. Polym. Environ. 26 (2018) 1239–1252.

652   https://doi.org/10.1007/s10924-017-1030-5.

653   [51]   Ó.L. Ramos, J.C. Fernandes, S.I. Silva, M.E. Pintado, F.X. Malcata, Edible Films and

654   Coatings from Whey Proteins: A Review on Formulation, and on Mechanical and Bioactive

655   Properties, Crit. Rev. Food Sci. Nutr. 52 (2012) 533–552.

656   https://doi.org/10.1080/10408398.2010.500528.

657   [52]   J.-W. Rhim, H.-M. Park, C.-S. Ha, Bio-nanocomposites for food packaging applications,

658   Prog. Polym. Sci. 38 (2013) 1629–1652. https://doi.org/10.1016/j.progpolymsci.2013.05.008.

659 [53] S.Y. Ooi, I. Ahmad, M.C.I.M. Amin, Cellulose nanocrystals extracted from rice husks as a

660 reinforcing material in gelatin hydrogels for use in controlled drug delivery systems, Ind.

661 Crops Prod. 93 (2016) 227–234. https://doi.org/10.1016/j.indcrop.2015.11.082.

662 [54] T.M. Santos, M.D.S.M. Souza Filho, C.A. Caceres, M.F. Rosa, J.P.S. Morais, A.M.B. Pinto,

663 H.M.C. Azeredo, Fish gelatin films as affected by cellulose whiskers and sonication, Food

664 Hydrocoll. 41 (2014) 113–118. https://doi.org/10.1016/j.foodhyd.2014.04.001.

665 [55] M.R.E. Santos, A.C. Fonseca, P. V. Mendonça, R. Branco, A.C. Serra, P. V. Morais, J.F.J.

666 Coelho, Recent developments in antimicrobial polymers: A review, Materials (Basel). 9

667 (2016). https://doi.org/10.3390/MA9070599.

668 [56] M. Ahmad, S. Benjakul, T. Prodpran, T.W. Agustini, Physico-mechanical and antimicrobial

669 properties of gelatin film from the skin of unicorn leatherjacket incorporated with essential

670 oils, Food Hydrocoll. 28 (2012) 189–199. https://doi.org/10.1016/j.foodhyd.2011.12.003.

671 [57] J. Wang, Y.P. Chen, K. Yao, P.A. Wilbon, W. Zhang, L. Ren, J. Zhou, M. Nagarkatti, C.

672 Wang, F. Chu, X. He, A.W. Decho, C. Tang, Robust antimicrobial compounds and polymers

673 derived from natural resin acids, Chem. Commun. 48 (2012) 916–918.

674 https://doi.org/10.1039/c1cc16432e.

675 [58] A. Cagri, Z. Ustunol, E.T. Ryser, Antimicrobial, mechanical, and moisture barrier properties

676 of low pH whey protein-based edible films containing p-aminobenzoic or sorbic acids, J.

677 Food Sci. 66 (2001) 865–870. https://doi.org/10.1111/j.1365-2621.2001.tb15188.x.

678